ELSEVIER

Journal of Fluids and Structures 24 (2008) 833–854

JOURNAL OF FLUIDS AND STRUCTURES

www.elsevier.com/locate/jfs

On the effect of spacing on the vortex-induced vibrations of two tandem cylinders

G.V. Papaioannou[a], D.K.P. Yue[a], M.S. Triantafyllou[a], G.E. Karniadakis[a,b,*]

[a]*Department of Mechanical Engineering, Massachusetts Institute of Technology, 77 Massachusetts Avenue, Cambridge, MA 02139, USA*
[b]*Division of Applied Mathematics, Brown University, 37 Manning Street, Providence, RI 02912, USA*

Received 8 May 2007; accepted 29 November 2007
Available online 18 April 2008

Abstract

A spectral element method using Jacobi polynomial bases is employed to study the vortex-induced oscillations of two identical elastically mounted cylinders in tandem arrangement. Three different cylinder spacings, $P/D = 2.5$, 3.5 and 5.0, are examined in order to identify the effect of spacing on the two-degree-of-freedom oscillations of the cylinders. Computations were conducted in two space dimensions (2-D)—an assumption that is expected to be valid for the Reynolds number, $\mathrm{Re} = 160$, considered. The single cylinder case is also examined at the same flow and structural parameters for reference and comparison. A widening of the range of the response region of the upstream cylinder is observed when the cylinder spacing is decreased. The synchronization curves of the upstream cylinder display a shift on the reduced velocity (V_R) axis depending on the spacing. The maximum oscillation amplitude of the downstream cylinder increases when the cylinders are brought to a distance that the flow around the corresponding stationary system displays reattachment. There are three significant frequencies at the spectral responses: the shedding frequency of the stationary tandem system (f_o^{**}); the shedding frequency of a single cylinder (f_o^{*}); and the natural frequency of the mass-spring system describing the dynamics of the cylinders (f_N). The energy input of the flow on each cylinder is studied in terms of the line integral of the hydrodynamic force yielding the work, the phase angle between force and displacement at the prominent spectral frequency, and finally the lift in phase with velocity.

Keywords: Tandem cylinders; Lock-in; Vortex shedding; ALE; DNS

1. Introduction

Flow-induced oscillations of bluff bodies are a subject that has attracted a lot of attention because of its interesting fluid dynamics aspects, as well as for its engineering applications. The flow past an oscillating cylinder has been studied by various researchers in the past. Classic review papers on the topic are those of Sarpkaya (1979) and Bearman (1984). Useful resources on the subject are also the books by Blevins (1994) and Naudascher and Rockwell (2005). A cylinder in uniform cross flow exhibits large amplitude oscillations when the natural frequency of cylinder vibration (f_N) is close to the vortex-shedding frequency of the stationary cylinder. The cylinder then sheds vortices at that frequency and the

*Corresponding author at: Division of Applied Mathematics, Brown University, 37 Manning Street, Providence, RI 02912, USA. Tel.: +1 401 863 1217; fax: +1 401 863 3369.
E-mail address: gk@dam.brown.edu (G.E. Karniadakis).

0889-9746/$ - see front matter © 2007 Elsevier Ltd. All rights reserved.
doi:10.1016/j.jfluidstructs.2007.11.006

condition is called 'lock-in'. The interaction of two cylinders arises in many engineering applications, including arrays of offshore risers and moorings, power transmission lines, suspension bridges and heat exchangers.

A number of distinct flow regimes exist depending on the separation distance and arrangement (Zdravkovich, 1987; Igarashi, 1981). For stationary cylinders in tandem arrangement, there are three main flow regimes but a further sub-categorization is possible. In very close proximity, the two cylinders behave as a single body. The shear layers emanating from the upstream cylinder roll-up after the downstream, forming a single wake. Increasing the cylinder spacing causes the shear layers emanating from the upstream cylinder to reattach on the downstream cylinder. The time-averaged force on the downstream cylinder has a component opposite to the free stream, and the shedding frequency reduces. When the cylinder spacing is increased beyond a critical spacing, vortex shedding occurs in the gap region between the two cylinders. The wake behind the cylinders consists of the combined wakes of the two cylinders and this regime is called *binary-vortex regime*.

Zdravkovich (1985) studied the flow-induced oscillations of two interfering, rigid, elastically supported circular cylinders for Reynolds numbers in the range 10^4–10^5. Two mechanisms of excitation were discussed: *Vortex-shedding excitation* and *fluid-elastic excitation*. The obtained data show that the synchronization range decreases as the cylinder separation increases. The critical velocity is considerably bigger in the reattachment regime compared to the binary-vortex regime cases. The reduced velocities triggering fluid-elastic excitation were significantly bigger than those triggering vortex-shedding excitation.

Laneville and Brika (1997) conducted experimental studies on the power imparted by wind to a flexible circular cylinder vibrating in the wake of a fixed upstream cylinder for different cylinder arrangements and spacings. The power input on the downstream cylinder decreased with increasing cylinder separation. Brika and Laneville (1999) have also investigated experimentally the dynamic response of a long flexible circular cylinder in the wake of a stationary geometrically similar cylinder at a low damping ratio. The separations they investigated range from 7 to 25 diameters and the Reynolds number ranged from 5000 to 27 000. For the tandem cylinders, their results indicated that: (a) the dynamic response of the downstream cylinder is no longer hysteretic, (b) the synchronization onset is at higher reduced velocities and (c) the synchronization region is wider than that of an isolated cylinder. For separation distances of 7 and 8.5 diameters, they found that the leeward cylinder exhibits a combination of vortex-induced and wake-galloping oscillations.

Hover and Triantafyllou (2001) studied the galloping response of a cylinder in the wake of a stationary cylinder of the same size. The cylinder was placed at a distance 4.75 diameters, both in-line and in 12° staggered arrangement at $\mathrm{Re} = 3 \times 10^4$. The results indicated that frequency lock-in occurs at a low reduced velocity and remains through $V_{rn} = 17$, but the phase change, which typically accompanies frequency lock-in, occurs at higher speeds. This phase change was claimed to be of the same nature as for single-cylinder tests.

Mittal and Kumar (2001) employed a stabilized finite-element formulation to study flow-induced oscillations of two cylinders in tandem and staggered arrangements for $\mathrm{Re} = 100$. In both arrangements the horizontal distance of the cylinders was 5.5 times the diameter. In almost all the cases, the upstream cylinder responded like an isolated single cylinder. Soft lock-in was observed in many cases. The vortex-shedding frequency of the cylinders was detuned from the structural frequency. They attributed the detuning to the relatively low mass ratio of each of the two cylinders which was $m^* = 4.7273$. They argued that as the mass of the oscillator increases, the detuning between the two frequencies reduces until eventually lock-in is observed. The structural damping coefficient they used was $\zeta = 3.3 \times 10^{-4}$.

Allen and Henning (2003) conducted current tank tests to study vortex-induced vibrations on two tandem cylinders in uniform as well as in shear flow at subcritical Reynolds numbers. They reported that, when the separation distance was sufficiently large, the downstream cylinder vibration exhibited frequencies at both the vibration frequency of the upstream cylinder and at a second, lower frequency equal to about 60–75% of the first.

Lam and To (2003) investigated experimentally the interference effect of a cylinder placed upstream of a smaller, flexibly mounted circular cylinder. Vibration response curves of the smaller cylinder were obtained at 64 relative arrangement positions of the two cylinders, including tandem, side-by-side, proximity, and staggered arrangements. For the tandem arrangements they found that for spacings up to 2.34 times the larger diameter, the flexible cylinder exhibits negligibly small oscillations at all reduced velocities, due to shielding by the larger cylinder upstream. For relatively large spacings, some obvious vibrations were found to occur at reduced velocity $V_R = 12$.

Assi et al. (2006) have recently presented an experimental study on the flow-induced oscillations of circular cylinders in tandem arrangement. The oscillations were limited to the transverse direction, but with quite low damping parameter $\zeta = 0.008$–0.0109. The Reynolds number of their experiments ranged between 3000 and 13 000 and reduced velocity varied up to 12. The center-to-center spacings they examined ranged between 2 and 5.6 diameters and the mass ratios m^* between 1 and 2.

In the present work, we study numerically the effect of spacing on the vortex-induced vibrations of two tandem cylinders. Three spacings are selected, $P/D = 2.5$, 3.5 and 5.0. Fig. 1 shows instantaneous vorticity visualization of the flow around the stationary tandem system at each spacing, as well as the stationary single cylinder. The first spacing

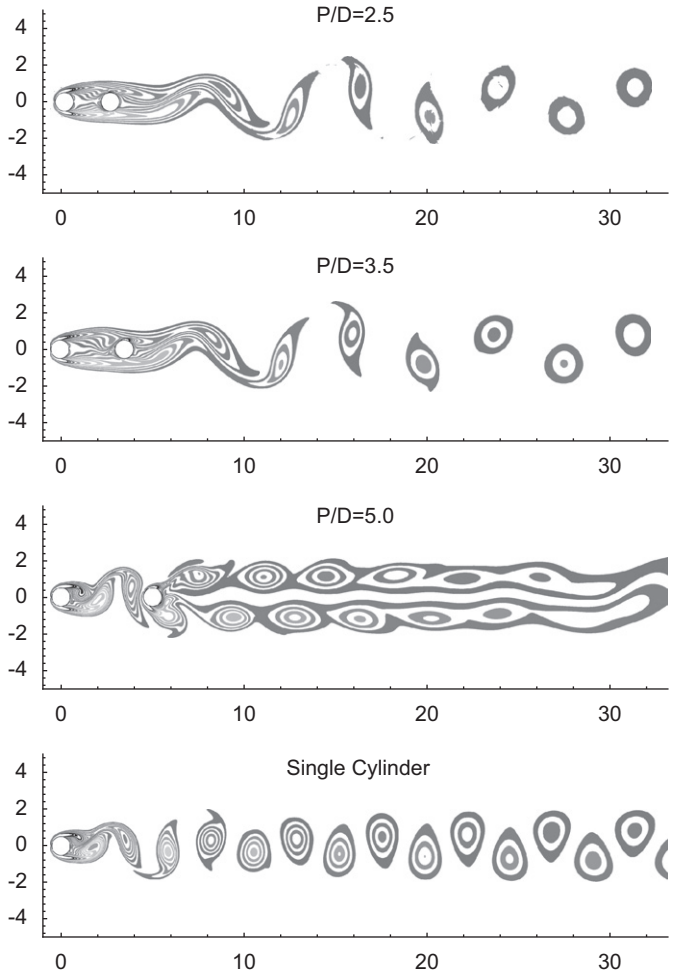

Fig. 1. Instantaneous visualization of flow around stationary cylinders. From top to bottom: tandem cases $P/D = 2.5$, 3.5, and 5.0; and single cylinder.

($P/D = 2.5$) belongs to the reattachment regime in the non-oscillating system. The last ($P/D = 5.0$) leads the corresponding stationary system to binary-vortex shedding. Finally, the spacing $P/D = 3.5$ is very close to the critical spacing of transition from reattachment to binary-vortex regime. In fact, due to a known hysteresis effect, this spacing is capable of sustaining flow with vortex shedding in the gap region, once such situation was somehow initiated. For more information on the hysteresis effect, the reader can refer to the original experimental work of Zdravkovich (1987), the numerical findings of Papaioannou (2003) and Jester and Kallinderis (2003). The single cylinder case is studied for the same structural parameters and Reynolds number for reference and comparison.

The paper is organized as follows. In Section 2, we outline the formulation and numerical procedure of the solution. The computational mesh and the simulation parameters are also described. In Section 3, we elaborate on the two-degree-of-freedom vortex-induced vibrations of the tandem cylinders. Transverse and in-line oscillation amplitudes, forces as well as dominant response frequencies are discussed. Hydrodynamic work is also analyzed and flow patterns are displayed. The conclusions and summary of the work are presented in Section 4.

2. Method and formulation

2.1. Flow formulation

An arbitrary Lagrangian–Eulerian (ALE) formulation of the incompressible Navier–Stokes equations is employed, as proposed by Hughes et al. (1981) and Donea et al. (1982). The mesh velocity will be denoted by $\hat{v}$ and is a field

variable. The equations describing the flow on a moving domain of reference ($\hat{x}$) can be written as

$$u_{i,t} + (u_j - \hat{v}_j)u_{i,j} = -p^*_{,i} + \mathrm{Re}^{-1}u_{i,jj}, \tag{1}$$

subject to the incompressibility condition,

$$u_{i,i} = 0. \tag{2}$$

The method of spectral elements on hybrid unstructured meshes, as explained in Karniadakis and Sherwin (2005), is employed for the spatial approximation of the solution.

For the time integration of Eqs. (1) and (2), the stiffly stable integration scheme of Karniadakis et al. (1991) is used suitably adapted for the staggered integration of the structure and flow domain equations, as follows.

(i) The position of the mesh nodes is updated taking into account the previously calculated mesh velocities ($\hat{v}_i$)

$$\frac{\gamma_0\hat{x}^{(n+1)} - \sum_{q=0}^{J_i-1}\alpha_q\hat{x}_i^{(n-q)}}{\Delta t} = \sum_{q=0}^{J_e-1}\beta_q\hat{v}_i^{(n-q)}, \tag{3}$$

where the values of α_q, β_q, and γ_0 can be found in Table 1.

(ii) The nonlinear terms are calculated and integrated to get

$$\frac{u_i^{n+1/3} - \sum_{q=0}^{J_i-1}\alpha_q u_i^{n-q}}{\Delta t} = \sum_{q=0}^{J_e-1}\beta_q[(u_j - \hat{v}_j)u_{i,j}]^{n-q}, \tag{4}$$

obtaining the first ($u_i^{(n+1/3)}$) of the three updates of the velocity field of the fractional step scheme.

(iii) Incompressibility is enforced in the next sub-step

$$\frac{u_i^{(n+2/3)} - u_i^{(n+1/3)}}{\Delta t} = -p^{*(n+1/2)}_{,i},\ u_{i,i}^{(n+2/3)} = 0. \tag{5,6}$$

Applying the gradient on (5) and enforcing (6), a Poisson equation for the pressure is obtained

$$p^{*(n+1/2)}_{,ii} = \frac{u_{i,i}^{(n+1/3)}}{\Delta t}. \tag{7}$$

For the solution of (7) a modified version of the pressure boundary conditions suggested in Karniadakis et al. (1991) is employed

$$p^*_{,i}n_i = n_i\left[\sum_{q=0}^{J_e-1}\beta_q(N(u_i,\hat{v}_i)^{(n-q)} + \mathrm{Re}^{-1}L(u_i)^{(n-q)}) + \ddot{q}_i^{(n-q)}\right], \tag{8}$$

where $N(u_i,\hat{v}_i) = (u_j - \hat{v}_j)u_{i,j}$ are the nonlinear terms in the ALE formulation, $L(u_i) = \varepsilon_{ijk}\varepsilon_{klm}u_{m,lj}$ is the Laplacian operator of the viscous terms, and $\ddot{q}_i$ the acceleration of the cylinder in contact with the portion of fluid boundary where the boundary condition is imposed. Once $p^{*(n+1/2)}$ has been found, Eq. (5) is used to obtain the updated velocity $u_i^{(n+2/3)}$.

(iv) The dynamic equations of each structure are solved using the method of *average acceleration*, as will be outlined in Section 2.3, and the new state vector $[q_i, \dot{q}_i, \ddot{q}_i]^{(n+1)}$ of each cylinder is obtained.

Table 1
Coefficients for stiffly stable schemes

Coefficient	$\mathcal{O}(1)$	$\mathcal{O}(2)$	$\mathcal{O}(3)$
α_0	1	2	3
α_1	0	$-\frac{1}{2}$	$-\frac{3}{2}$
α_2	0	0	$\frac{1}{3}$
γ_0	1	$\frac{3}{2}$	$\frac{11}{6}$
β_0	1	2	3
β_1	0	-1	-3
β_2	0	0	1

(v) The viscous correction is then found

$$\frac{\gamma_0 u_i^{(n+1)} - u_i^{(n+2/3)}}{\Delta t} = \frac{u_{i,jj}^{(n+1)}}{\mathrm{Re}}. \tag{9}$$

The velocity boundary condition for Eq. (9) on the portion of the boundary corresponding to a moving cylinder is

$$u_i^{(n+1)} = \dot{q}_i^{(n+1)}, \tag{10}$$

where $\dot{q}_i^{(n+1)}$ is the updated velocity vector of the cylinder in contact with the fluid boundary where the condition is imposed.

(vi) The new velocity of the mesh is then calculated by solving

$$(\tilde{k}(x_i)\hat{v}_{i,j}^{(n+1)})_{,j} = 0, \tag{11}$$

where $\tilde{k}$ denotes an arbitrarily defined function that allows for an indirect local control of the mesh velocity. The boundary conditions for (11) are $\hat{v}^{(n+1)} = 0$ on the external boundaries of the mesh, and

$$\hat{v}_i^{(n+1)} = \dot{q}_i^{(n+1)}, \tag{12}$$

on flow mesh boundaries in contact with moving bodies.

(vii) At the end of each time step, the force vector on each moving body is calculated taking into account the pressure distribution and viscous stresses:

$$F_k^{(n+1)} = \oint_{\Gamma_{\mathrm{cyl}}} \left(-p^{*(n+1/2)}\delta_{jk} + \frac{1}{\mathrm{Re}}(u_{k,j}^{(n+1)} + u_{j,k}^{(n+1)}) \right) n_j \, \mathrm{d}s, \tag{13}$$

where n_j is the unit vector normal to the cylinder boundary Γ_{cyl}. This will be needed in the next iteration when the dynamic equations for the structures are found.

2.2. Computational domain

Hybrid meshes consisting of quadrilaterals and triangles are used. The number of triangular and quadrilateral elements for each case is summarized in Table 2. For consistency among the different spacings considered, the outer part of the mesh is kept the same in all examined cases. Each mesh is 24 diameters wide and 58 diameters long as seen in Fig. 2 for the single cylinder. The center of the upstream cylinder is used as the origin of the coordinate system. An inner mesh block $[-2.0, 7.5] \times [-4.0, 4.0]$ is substituted for each different spacing as seen in Fig. 3.

2.3. Structural model

The governing equations for the dynamic response of each body are

$$m^* \ddot{q}_i^* + c^* \dot{q}_i^* + k^* q^* = F_i^*, \tag{14}$$

where $q_i^* = q_i/D$ is the vector of displacement nondimensionalized by the cylinder diameter, and $m^* = m/(\rho D^2)$, $c^* = c/(\rho D U_\infty)$, and $k^* = k/(\rho U_\infty^2)$ are the nondimensional mass ratio, damping coefficient, and stiffness constant, respectively. Time is nondimensionalized by D/U_∞ and the force as $F^*/(\rho D U_\infty^2)$. All calculations that follow involve

Table 2
Number of triangular (N_{EL}^{tri}) and quadrilateral (N_{EL}^{quad}) elements, and total number of elements (N_{EL}) for each hybrid computational mesh

Case	N_{EL}	N_{EL}^{tri}	N_{EL}^{quad}	M^{tri}	M^{quad}
Single cylinder	1824	618	1206	21	36
$P/D = 2.5$	1748	722	1026	28	49
$P/D = 3.5$	1816	790	1026	28	49
$P/D = 5.0$	1966	940	1026	28	49

Also, total number of modes per triangular (M^{tri}) and per quadrilateral element (M^{quad}).

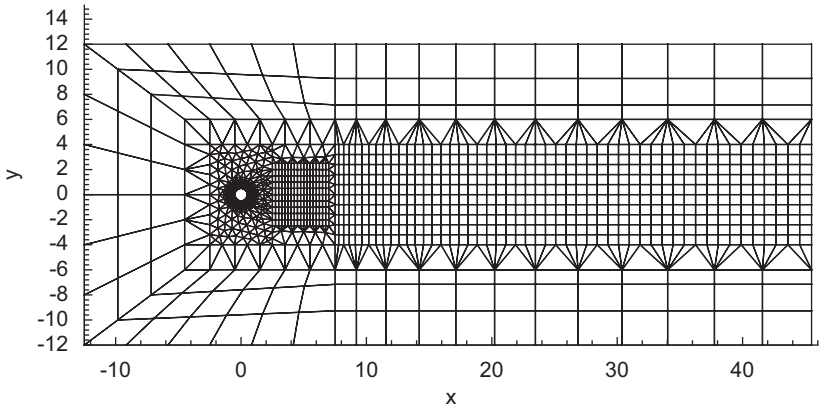

Fig. 2. Computational mesh for single cylinder.

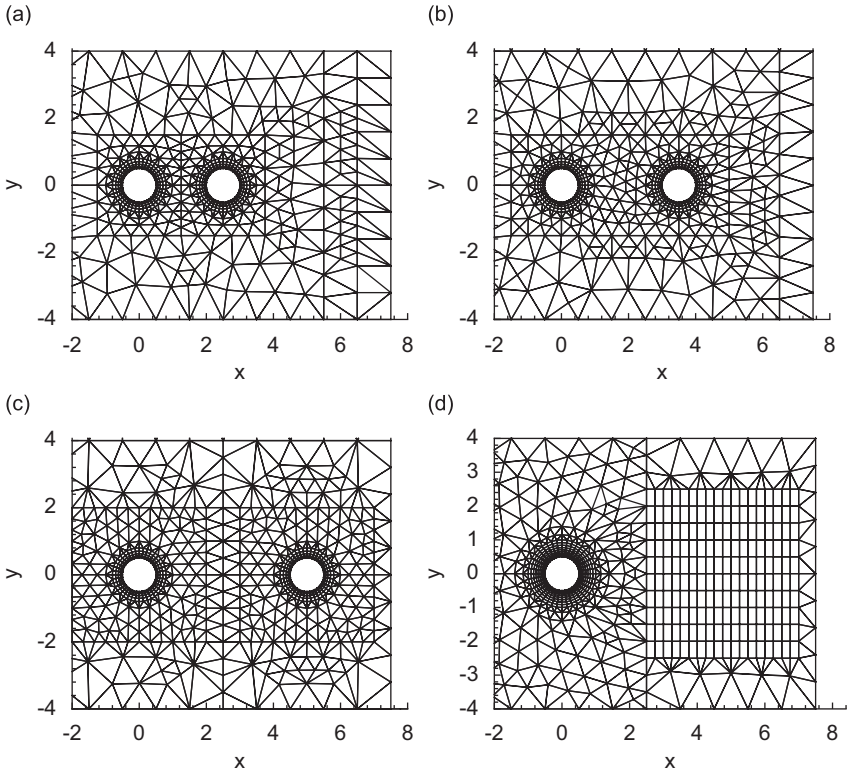

Fig. 3. Close-up zoom of computational meshes for: (a) tandem cylinders at spacing $P/D = 2.5$; (b) tandem cylinders at spacing $P/D = 3.5$; (c) tandem cylinders at spacing $P/D = 5.0$; (d) single cylinder.

the nondimensional quantities and for brevity we will drop the asterisks in these quantities. The natural frequency of such an oscillator in vacuum is

$$\omega_{NA} = \sqrt{\frac{k}{m} - \left(\frac{c}{2m}\right)^2}. \tag{15}$$

Typically, $k/m \gg (c/2m)^2$. Eq. (14) can be rewritten in terms of a nominal natural frequency, $f_N = (1/2\pi)(k/m)^{1/2}$,

$$\ddot{q}_i + 2\zeta_s \omega_N \dot{q}_i + \omega_N^2 q_i = \frac{F_i}{m}. \tag{16}$$

The forcing term is the hydrodynamic force acting on each cylinder.

Despite its linearity, Eq. (16) is complicated due to the dependence of the hydrodynamic force on the displacement (q), the velocity ($\dot{q}$) and the acceleration ($\ddot{q}$). Eq. (16) is solved numerically using the method of average acceleration, a member of the Newmark family (Newmark, 1959). In its general form, the Newmark iteration is written as

$$\begin{aligned} &\ddot{q}^{n+1} + 2\zeta_s \omega_N \dot{q}^{n+1} + \omega_N^2 q^{n+1} = F^{n+1}/m, \\ &q^{n+1} = q^n + \Delta t \dot{q}_i^n + \frac{\Delta t^2}{2}[(1-2\beta)\ddot{q}_i^n + 2\beta \ddot{q}_i^{n+1}], \\ &\dot{q}^{n+1} = \dot{q}^n + \Delta t[(1-\gamma)\ddot{q}^n + \gamma \ddot{q}^{n+1}]. \end{aligned} \tag{17}$$

When integrating only for the structure with an *a priori* known $F^{(n+1)}$ this method is unconditionally stable for $2\beta \geqslant \gamma \geqslant 0.5$. The method of average acceleration used here is obtained for $\beta = 0.25$ and $\gamma = 0.5$.

2.4. Simulation parameters and initial conditions

A time step $\Delta t = 0.001$ is used for all the tandem cases simulations, while for a single cylinder the time step used is $\Delta t = 0.002$. We performed several temporal and spatial resolution tests before we arrive at these discretization parameters.

For each set of numerical simulations, the solution of the stationary tandem cylinders for the corresponding spacing was used as initial condition. This consistent way of initializing the run for different reduced velocities leads to results on the same branch of possible hysteretic effects.

A mass ratio $m^* = 10$ and a damping parameter $\zeta_S = 0.01$ were used, while the natural frequency $f_N = (1/2\pi)(k/m^*)^{1/2}$ was varied. In the present context the reduced velocity is defined $V_R = U_\infty / D f_N$. The reduced velocity (V_R) and the structural natural frequency f_N, which are inversely proportional, are alternatively used throughout the text.

3. Vortex-induced vibrations of two tandem cylinders

3.1. Effect of spacing on the amplitude and force responses

The spacing between the two cylinders is found to affect the two-degree-of-freedom oscillations of the tandem cylinders in a number of ways discussed in this section. The oscillations are predominantly in the transverse direction for all examined spacings, as well as for the single cylinder, in the range of reduced velocities considered. The cylinder trajectories for one of the lock-in cases, as well as a low reduced velocity V_R are plotted in Fig. 4. For relatively low values of V_R the oscillation amplitude of the downstream cylinder is much higher than that of the upstream, both in the in-line and transverse directions. The range of reduced velocities (V_R) considered does not cover the fluid-elastic excitation regime where in-line oscillations are in many cases dominating over transverse, as reported by Zdravkovich (1985). The in-line response is generally higher on the downstream than the upstream cylinder for almost the whole range of reduced velocities and cylinder spacings.

This is also seen in detail in Figs. 5 and 6, where we have plotted the variation of the maximum amplitude response in the vertical (A_Y) and horizontal (A_X) direction, respectively, with the reduced velocity (V_R), parametrically over the cylinder spacing (P/D). Each plot is horizontally divided in two plots. The left shows the response of the upstream cylinder, while the right for the downstream. The result of a single oscillating cylinder with similar structural characteristics is also included for comparison.

The response curve of the upstream cylinder shifts on the V_R axis as the cylinder spacing changes. This is illustrated better by Fig. 5(b) where the centerline of the synchronization curve is plotted. At any given amplitude up to the maximum of the synchronization curve a constant amplitude horizontal line intersects the curve in two points defining a reduced velocity interval. The mid-points of every such interval for amplitudes up to the maximum define the centerline of the curve. The shift is qualitatively consistent with the shift in the shedding frequency of the corresponding stationary system. Table 3 shows the values of the shedding frequency for the stationary system at the same Reynolds number examined, $\mathrm{Re} = 160$. The shedding frequency of the stationary tandem cylinders is minimum near the critical spacing [see also Papaioannou et al. (2006)]. As can be seen in the left side of Fig. 5, the orders of both the increasing part of the

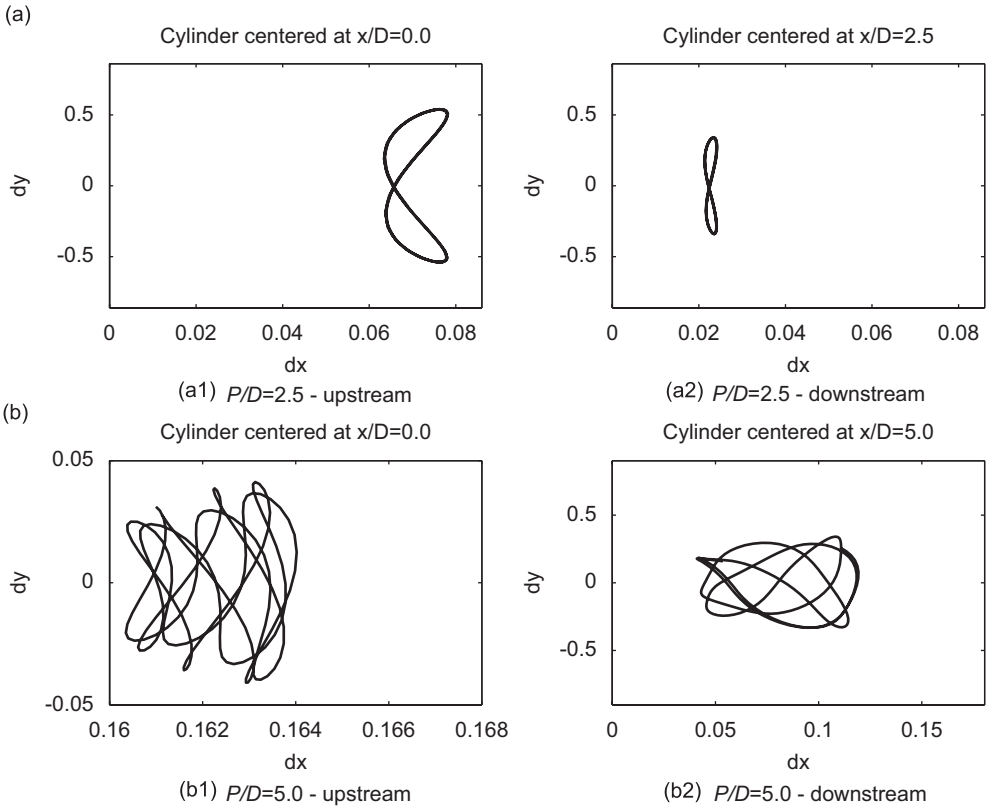

Fig. 4. Cylinder trajectories for: (a) spacing $P/D = 2.5$ and reduced velocity $V_R = 5.5$, axes ratio 20:1; (b) spacing $P/D = 5.0$ and reduced velocity $V_R = 10.0$.

response curves up to the peak value, as well as the centerline, are consistent with the order of the corresponding stationary shedding frequency (f_o^{**}).

As spacing is reduced, the response curve width, in terms of reduced velocities (V_R), of the upstream cylinder increases. This is more clearly illustrated in the left plot of Fig. 7. In this figure, the width of the synchronization curve is plotted for increasing terminal oscillation amplitudes. This finding is very likely related to the widening of the synchronization region observed in the forced cylinder oscillation experimental results of Mahir and Rockwell (1996). They compared the lock-in region between spacings $P/D = 2.5$ and 5.0 for forced oscillations and found that the width of the lock-on region increases. It should be noted, however, that the width increase on the upstream cylinder due to the presence of the downstream is less significant than other factors such as a change in mass ratio or damping parameter. As explained in Khalak and Williamson (1999), the width of the synchronization region for a single cylinder increases with reducing mass ration m^* and mass-damping parameter $m^*\zeta$. For the downstream cylinder the presence of the upstream has a more considerable effect.

The maximum, over the examined V_R range, transverse oscillation amplitude of the downstream cylinder, is higher for the cases $P/D = 2.5$ and 3.5 than for the case $P/D = 5.0$. However, for increasing reduced velocities the larger spacing ($P/D = 5.0$) case exhibits higher oscillation amplitudes both in the transverse and in-line directions.

The in-line response of the downstream cylinder presents at least two peaks in the range of reduced velocities examined. The first peak corresponds to the V_R of maximum in-line and transverse oscillations of the upstream cylinder, and it is therefore related to the vortex emanating from it. The second is at a higher V_R, coinciding with the maximum transverse oscillations of the downstream cylinder ($V_R = 6.67$), and can be related to the vortex shedding of the downstream cylinder under the action of the oncoming upstream cylinder wake. Two peaks are also present in the C'_D of the downstream cylinder.

Similarly, Figs. 8, 9 and 10 show the variation of the mean drag coefficient ($\overline{C_D}$), as well as the root-mean-square (rms) of the drag and lift coefficients (C'_D, C'_L), respectively. The figures are outlined as described in Figs. 5 and 6. The constant horizontal lines indicate the values of each cylinder at the stationary system for each spacing.

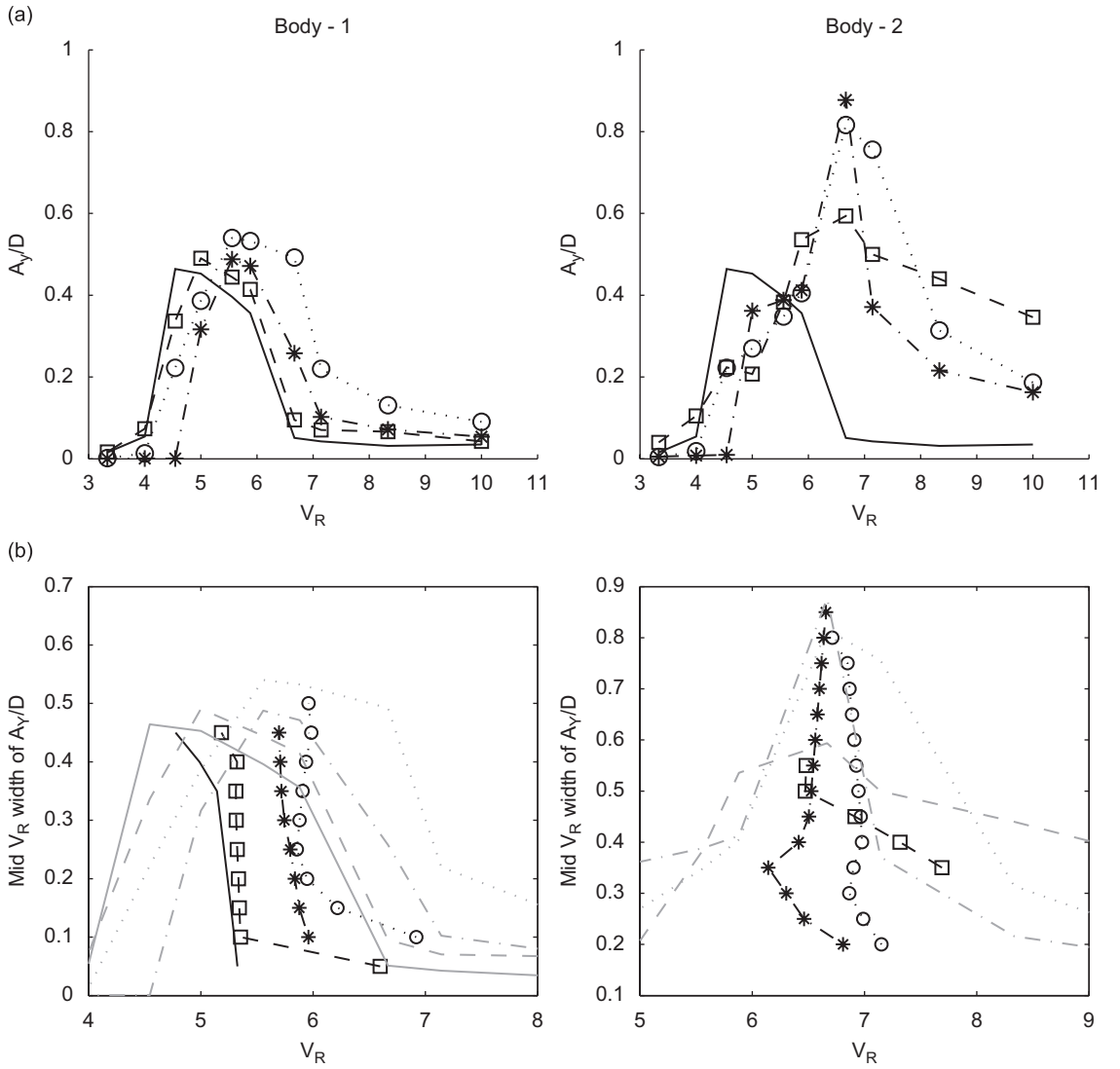

Fig. 5. Left: upstream cylinder; right: downstream cylinder. (a) Variation of vertical oscillation amplitude (A_Y) with V_R: ——, single cylinder; ⋯○⋯, tandem, $P/D = 2.5$; ---∗---, tandem, $P/D = 3.5$; −−□−−, tandem, $P/D = 5.0$. (b) Mid-V_R of vertical response (A_Y/D) width: ——, single cylinder; ⋯○⋯, tandem, $P/D = 2.5$; ---∗---, tandem, $P/D = 3.5$; −−□−−, tandem, $P/D = 5.0$.

When the reduced velocity (V_R) decreases away from the synchronization region the drag coefficient of both cylinders and for all examined spacings (P/D) resumes the value that corresponds to the stationary system. As shown in Figs. 5 and 6 the responses for $V_R < 3.5$ are very small. Thus, the flow topology at small reduced velocities resembles that of the stationary cylinders, as seen in Fig. 11 in comparison with Fig. 1, resulting in similar forces.

For V_R higher than those corresponding to vortex-induced synchronization, the $\overline{C_D}$ of the upstream cylinder is approximately the same for all three cylinder spacings examined; the same is true for the C'_L. This is observed because the oscillations corresponding to those reduced velocities are still large enough for all examined spacings, to allow vortex shedding in the gap region, as seen in Figs. 12 and 13. For stationary tandem cylinders we know that after vortex shedding in the gap region has taken place, the effect of the downstream cylinder on the upstream is vanishing.

The rms of the forces follow the corresponding variations in the response amplitude. But they also attain a common value when the V_R is large enough that the response on the upstream cylinder is very small for all spacings. Similarly to the single cylinder case, the mean drag coefficient of the upstream cylinder reaches a maximum at lock-in.

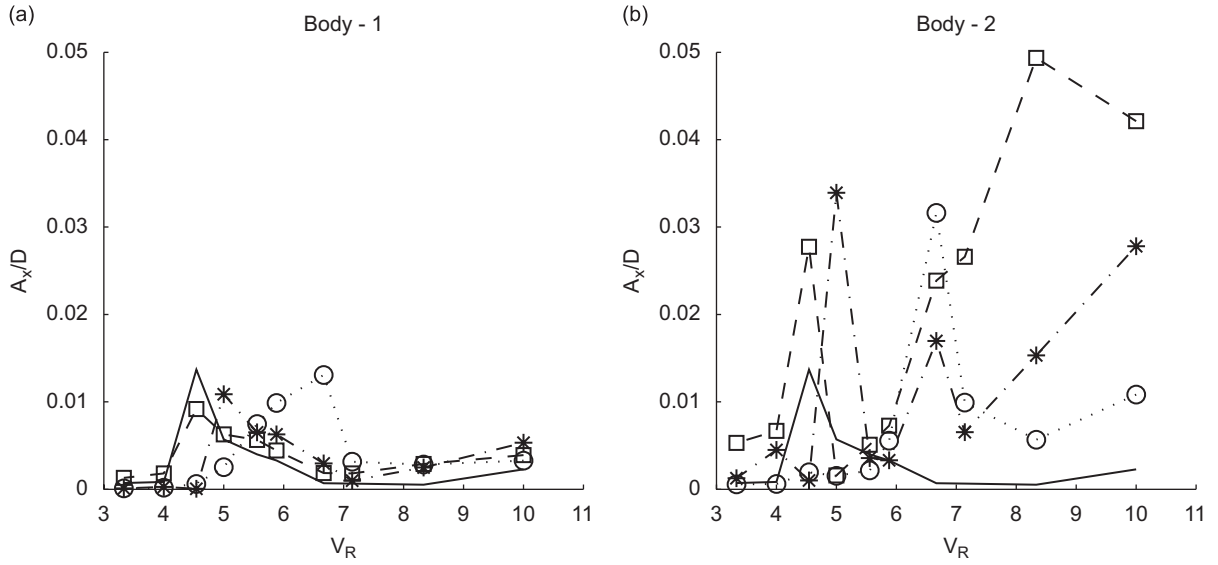

Fig. 6. Variation of horizontal oscillation amplitude (A_X) with reduced velocity (V_R) (a) for upstream cylinder, (b) for downstream cylinder: ——, single cylinder; · · · ○ · · ·, tandem, $P/D = 2.5$; ---∗---, tandem, $P/D = 3.5$; – –□– –, tandem, $P/D = 5.0$.

Table 3
Shedding frequencies of stationary tandem cylinders at $\mathrm{Re} = 160$

Case	f_o^*	Case	f_o^{**}
Single stand-alone	0.188	Tandem $P/D = 2.5$	0.128
		Tandem $P/D = 3.5$	0.124
		Tandem $P/D = 5.0$	0.176

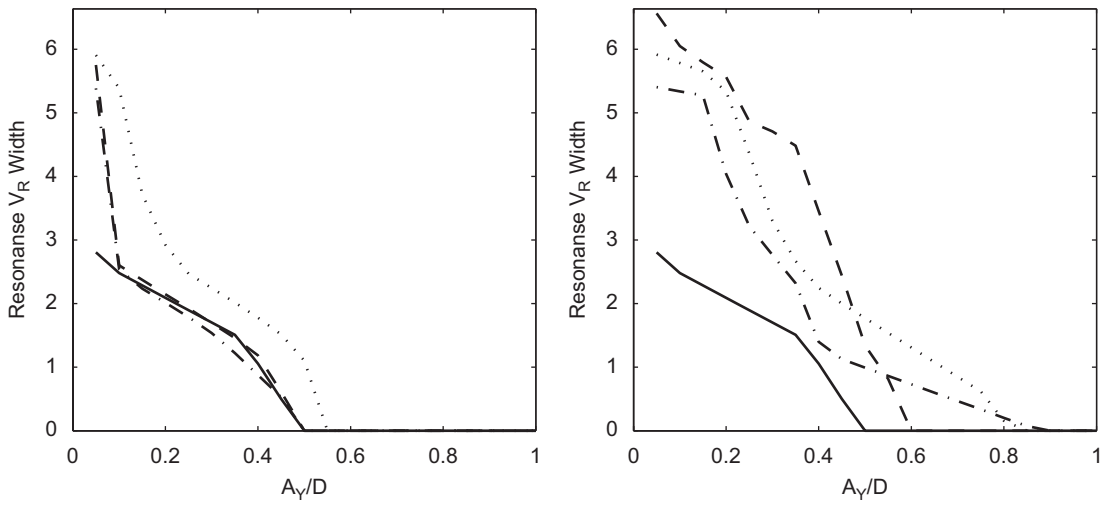

Fig. 7. Width of resonance V_R range as a function of the vertical response amplitude (A_Y). Left: for upstream cylinder; right: for downstream cylinder. ——, single cylinder; · · · · · ·, tandem, $P/D = 2.5$; -·-·-, tandem, $P/D = 3.5$; – – – –, tandem, $P/D = 5.0$.

The force and amplitude responses of the upstream cylinder in the $P/D = 5.0$ case are very close to that of the single cylinder. The effect of the downstream cylinder oscillation on the upstream for this spacing is relatively small.

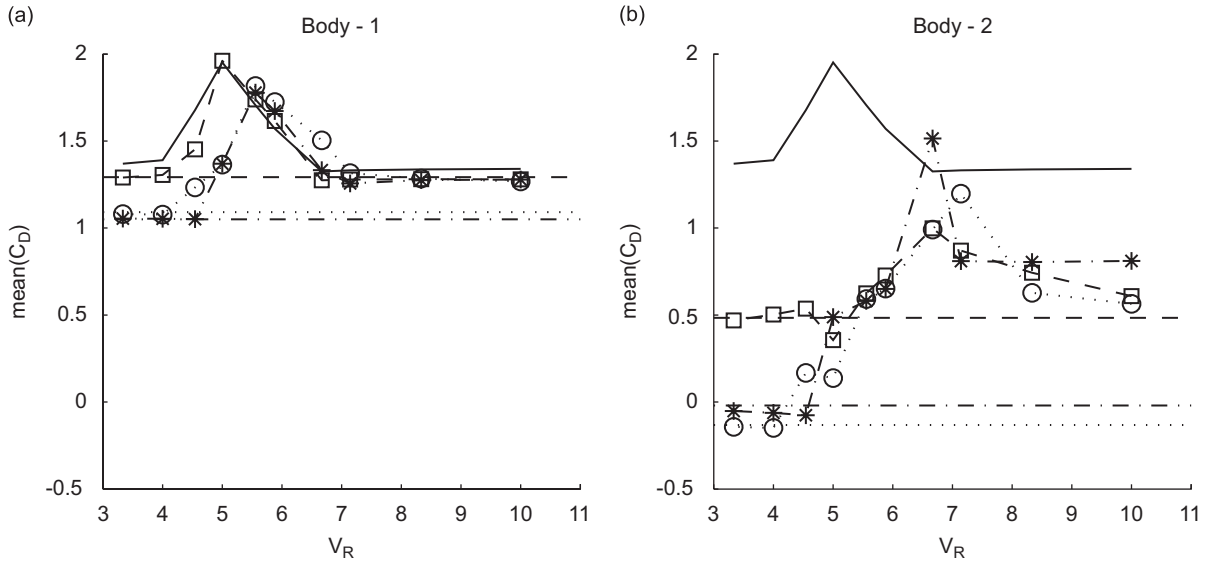

Fig. 8. Variation of mean drag coefficient ($\overline{C_D}$) with reduced velocity (V_R) (a) for upstream cylinder, (b) for downstream cylinder: ——, single cylinder; · · · ○ · · ·, tandem, $P/D = 2.5$; ---∗---, tandem, $P/D = 3.5$; – –□– –, tandem, $P/D = 5.0$; corresponding horizontal lines show the value of $\overline{C_D}$ for the stationary case at this spacing.

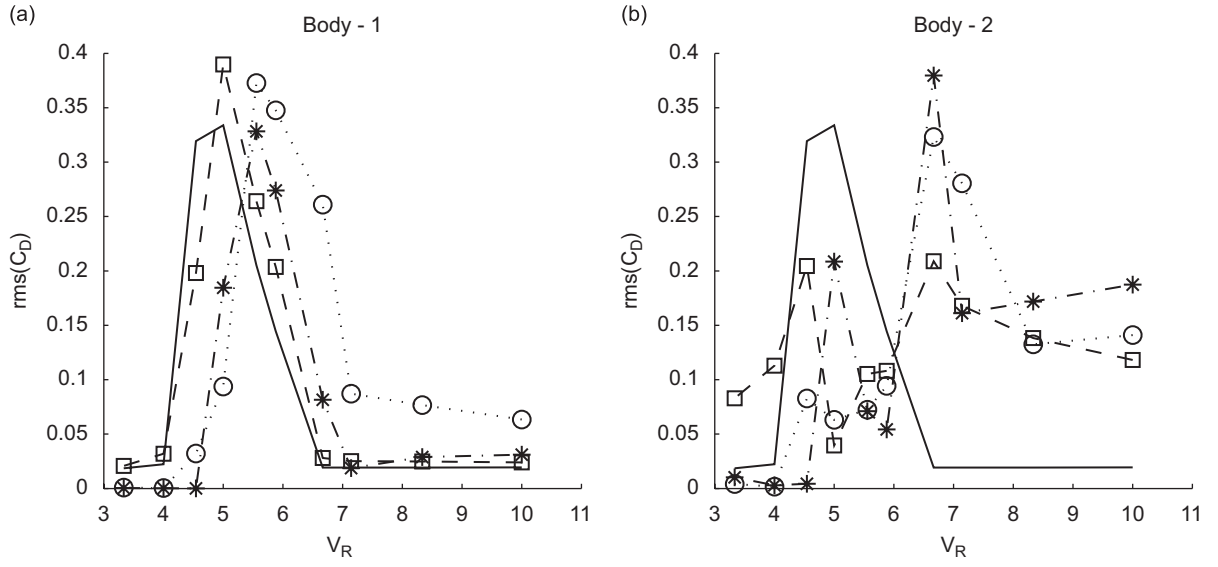

Fig. 9. Variation of rms-drag coefficient (C'_D) with reduced velocity (V_R) (a) for upstream cylinder, (b) for downstream cylinder: ——, single cylinder; · · · ○ · · ·, tandem, $P/D = 2.5$; ---∗---, tandem, $P/D = 3.5$; – –□– –, tandem, $P/D = 5.0$.

3.2. Spectral analysis of responses

Spectral analysis was conducted on the time-histories of the displacements and forces, in both the horizontal and vertical directions after elimination of transient response. Prominent peaks selection for each spacing and reduced velocity yielded the summary plot of Fig. 14 for the transverse displacement.

In Fig. 14, there are three plots corresponding to the different spacings $P/D = 2.5$, 3.5 and 5.0. Each plot contains the spectral peaks of the upstream and downstream cylinder for the corresponding case as well as those of the single

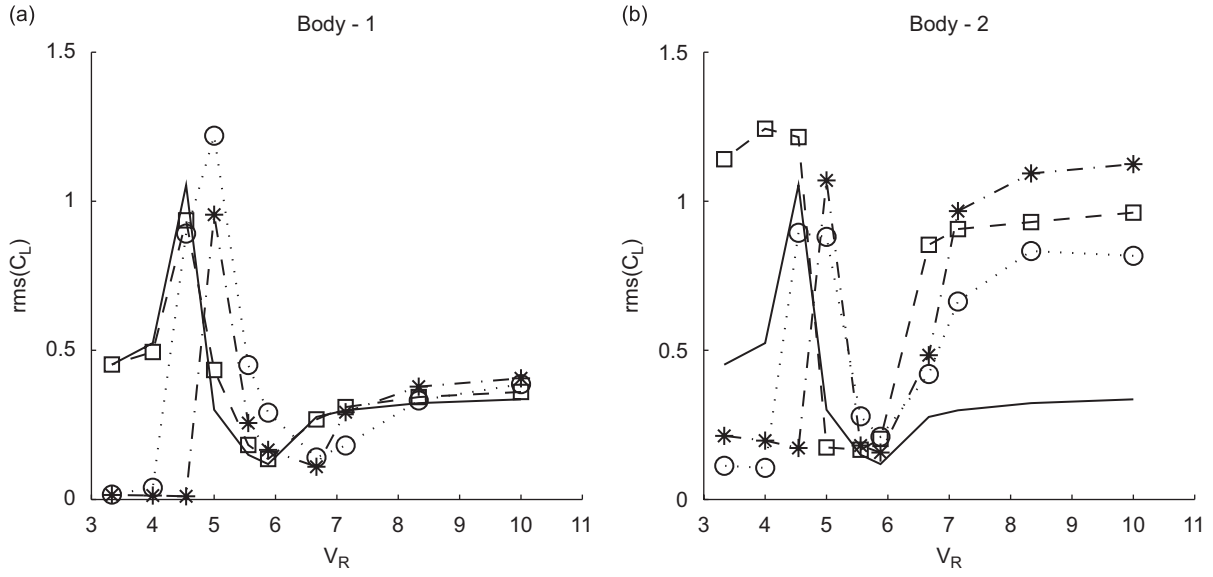

Fig. 10. Variation of rms-lift coefficient (C'_L) with reduced velocity (V_R) (a) for upstream cylinder, (b) for downstream cylinder: ——, single cylinder; · · · ○ · · ·, tandem, $P/D = 2.5$; ---∗---, tandem, $P/D = 3.5$; – –□– –, tandem, $P/D = 5.0$.

cylinder case. To help explain the peaks, diagonal lines corresponding to the shedding frequencies of the corresponding stationary tandem (f_o^{**}) and single cylinder (f_o^{*}) are plotted. Constant horizontal lines with unit ordinate indicate the natural shedding frequency of the structure f_N. Before discussing and interpreting the spectral peaks, it should be noted that the error on the frequency obtained by the fast Fourier transform is between 0.002 and 0.008 depending on the length of the available. There are three significant frequencies in the spectra. The natural frequency of the structure is f_N. The shedding frequency of the stationary tandem system is f_o^{**}, which depends on the spacing. And the shedding frequency of a single stationary cylinder f_o^{*} at the given Reynolds number.

For small values of the reduced velocity V_R (stiff spring), the prominent frequency of response is that of the corresponding stationary system (f_o^{**}). The oscillations exhibited by the cylinders are very small and the flow topology resembles that of the stationary case, as seen in Fig. 11, yielding vortex shedding at the corresponding frequency. Spectral peaks at the natural frequency of the structure f_N appear occasionally in the smaller spacing examined ($P/D = 2.5$) and at the upstream cylinder. This is not in the lock-in range, and other spectral peaks at characteristic frequencies of the system should not be unexpected.

At the synchronization (lock-in) range the spectral peaks follow the horizontal line. The vortex shedding is tuned at the natural frequency of the cylinders f_N. For the horizontal force and displacement the tuning occurs at twice the natural frequency of the cylinders $2f_N$. The widening in the synchronization range for the case $P/D = 2.5$ is also manifested here. There is wider range of reduced velocities V_R for which the peaks lie on the horizontal line corresponding to the natural frequency.

For reduced velocities higher than the synchronization range (soft spring) the cylinders respond at a frequency between the natural shedding frequency of the stationary system with the corresponding spacing (f_o^{**}) and the natural shedding frequency of the single cylinder (f_o^{*}). For the case $P/D = 2.5$ the response peaks of the vertical displacement lie very close to the diagonal corresponding to f_o^{**}. The same is true for the case $P/D = 5.0$ but for that spacing there are prominent peaks on the horizontal unit ordinate corresponding to the natural frequency of the cylinders f_N. The situation is somewhat different in the case $P/D = 3.5$ where the peaks lie away from the f_o^{**} diagonal and closer, but not exactly on, the f_o^{*} diagonal. The case $P/D = 3.5$ is just below the critical spacing for vortex shedding in the gap region. In fact, it is within the region where a known hysteresis effect occurs. Due to this hysteresis effect in this spacing even when the cylinders are stationary, vortex shedding in the gap region can be stably sustained once it is initiated. One of the ways to initiate such condition is the perturbation of the cylinders. Another way to initiate shedding in the gap region of the stationary system at $P/D = 3.5$ is by reducing to that spacing continuously starting from higher spacings, or start from higher Reynolds numbers and reduce. Small disturbances in the flow, like those caused by slight cylinder oscillation, cause vortex shedding in the gap region. At reduced velocities $V_R > 7$ the downstream cylinder exhibits

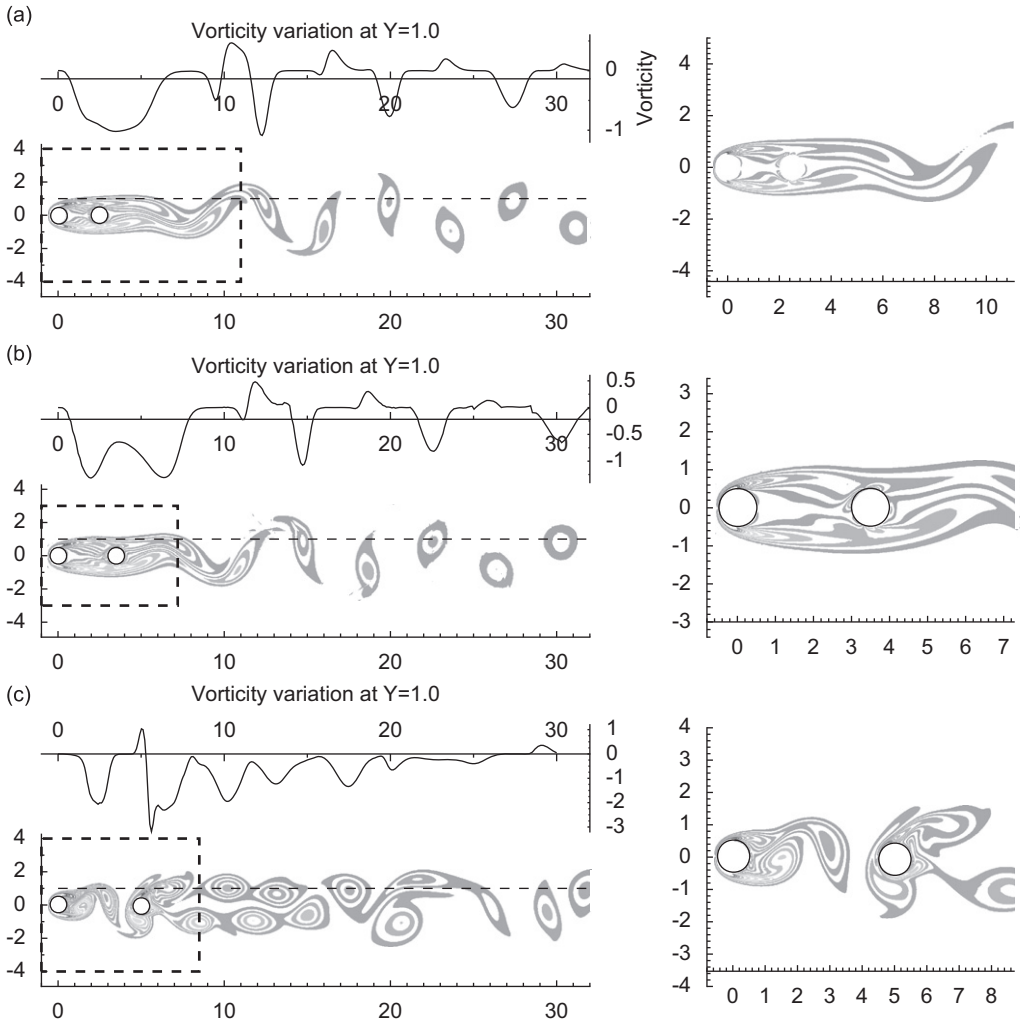

Fig. 11. Instantaneous vorticity fields corresponding to $V_R = 4.0$ for tandem cylinders at spacings: (a) $P/D = 2.5$; (b) $P/D = 3.5$; (c) $P/D = 5.0$. Variation of instantaneous vorticity along constant $y = 1.0$.

considerably higher oscillations than the upstream and the flow exhibits a pair of vortices in the gap region yielding responses closer to the f_o^* diagonal.

The spectral peaks of the single cylinder are repeated in each plot and are characterized by peaks on the f_o^* diagonal, followed by peaks on the horizontal corresponding to f_N during lock-in and then again peaks on the f_o^* diagonal.

3.3. Hydrodynamic work

The total work of the hydrodynamic force (W_T) on each cylinder undergoing two-degree-of-freedom oscillations is written as the line integral of the force over the cylinder trajectory and can be decomposed into the work in the in-line (x-) and transverse (y-) directions,

$$\oint F_i \, \mathrm{d}s_i = \frac{1}{N} \int_{x(kT)}^{x((k+N)T)} F_x \, \mathrm{d}x + \frac{1}{N} \int_{y(kT)}^{y((k+N)T)} F_y \, \mathrm{d}y. \tag{18}$$

The period entering Eq. (18) is based on the transverse oscillations. For more robust calculation an average over several (N) periods is obtained.

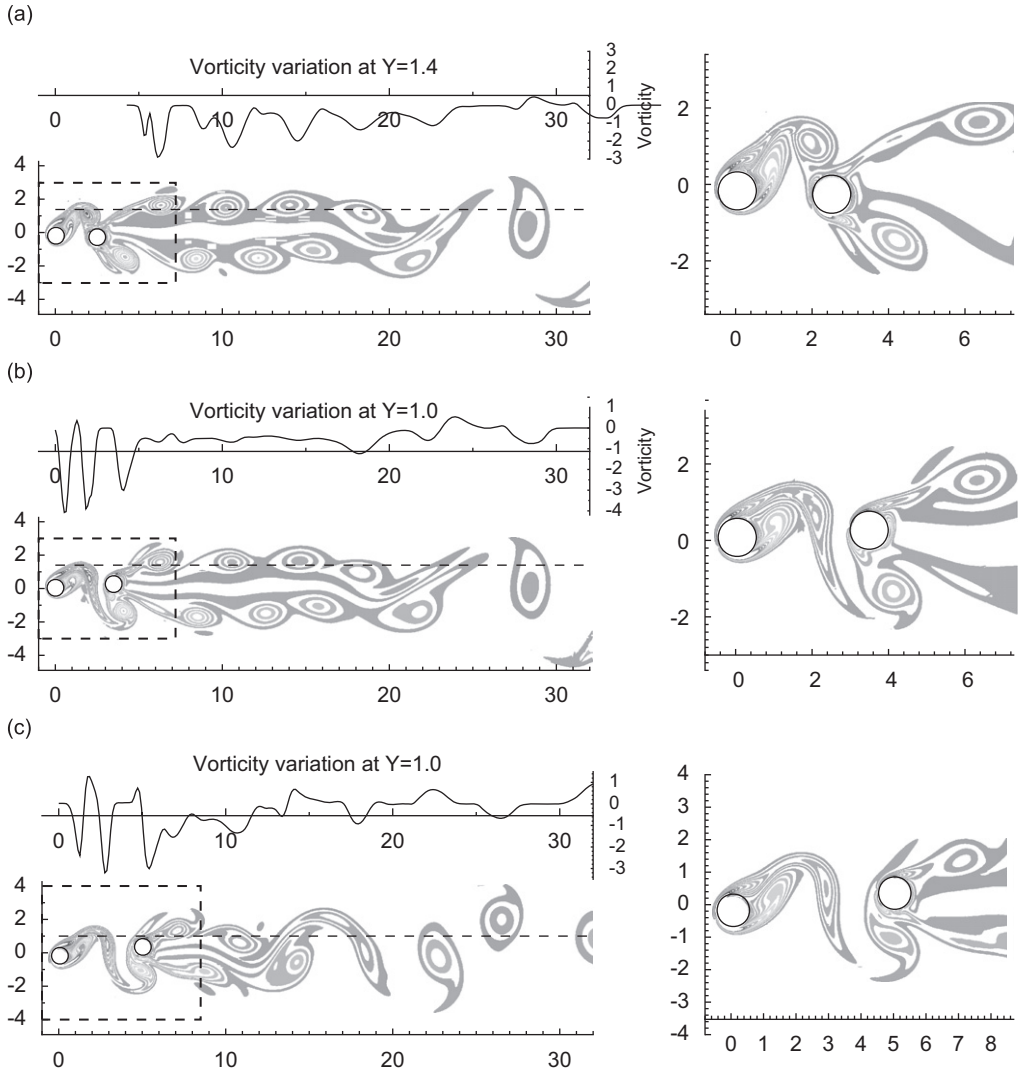

Fig. 12. Instantaneous vorticity fields corresponding to $V_R = 5.55$ for tandem cylinders at spacings: (a) $P/D = 2.5$; (b) $P/D = 3.5$; (c) $P/D = 5.0$. Variation of instantaneous vorticity along constant y.

In cases where more than one frequency peaks are present, trajectories do not form closed loops, averaging over several integer multiples of the prominent frequency produces an approximate average of the work input on the cylinder. In Fig. 15 the total hydrodynamic work on each cylinder is compared among different spacings. The work on a single cylinder is also presented for comparison.

The findings are consistent with the conclusions drawn by observation of the response amplitudes. The total hydrodynamic work has a higher maximum in the spacings corresponding to reattachment ($P/D = 2.5$ and 3.5) compared to the case $P/D = 5.0$ or the single cylinder. Those spacings also exhibit wider range of reduced velocities V_R for which the hydrodynamic force inputs work on the cylinder. The shifting of the curves on the V_R axis is also consistent with the earlier discussions on the amplitude responses.

The results presented in Fig. 15, based on Eq. (18), contain the contributions of all frequency components of the force and amplitude spectrum. Substituting the force and displacement by their Fourier series representations, we have

$$W = \mathscr{R}e\left\{\int_{t_1}^{t_2}\sum_{k=0}^{N-1} F_k e^{i(\omega_k t+\phi_k)}\,\mathrm{d}\left(\sum_{j=0}^{N-1} x_j e^{i\omega_j t}\right)\right\}, \tag{19}$$

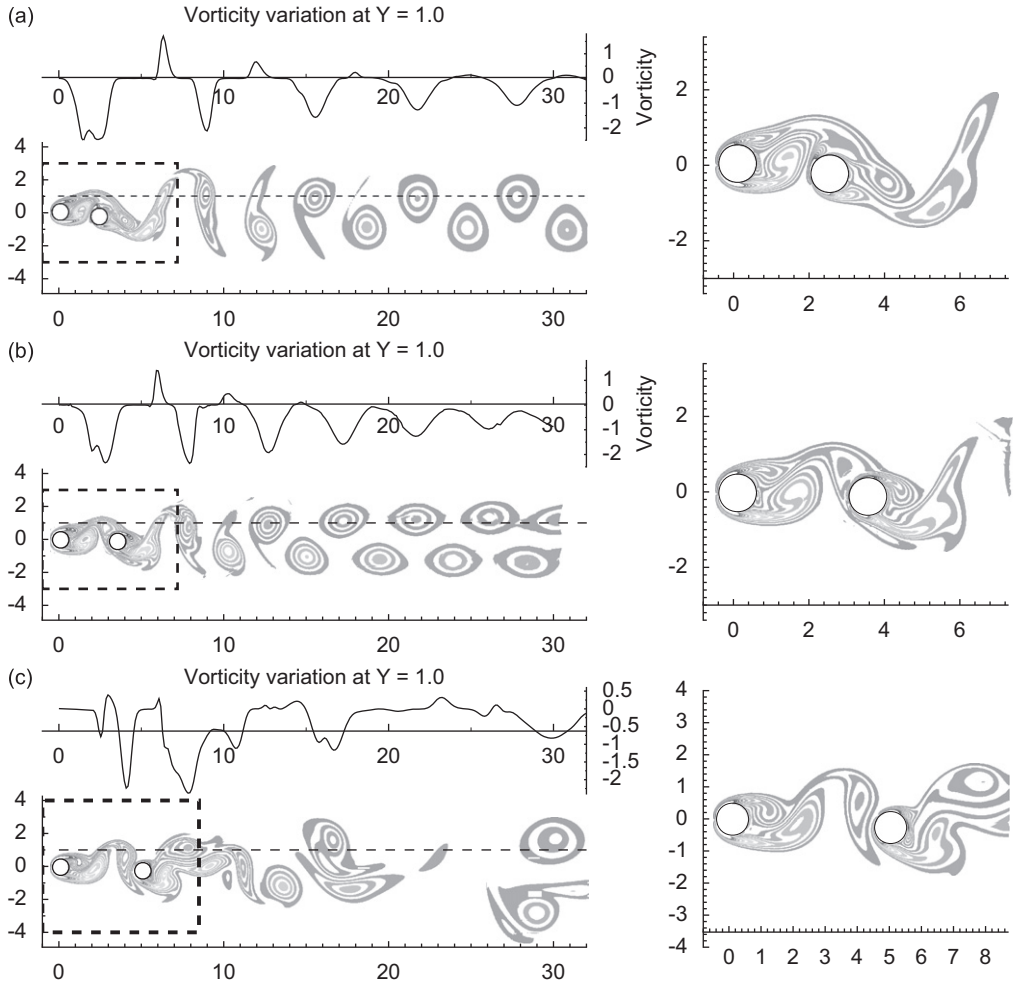

Fig. 13. Instantaneous vorticity fields corresponding to $V_R = 8.333$ for tandem cylinders at spacings: (a) $P/D = 2.5$; (b) $P/D = 3.5$; (c) $P/D = 5.0$. Variation of instantaneous vorticity along constant y.

from which we obtain

$$W = \mathscr{R}e\left\{\sum_{k=0}^{N-1}\sum_{j=0}^{N-1} F_k\omega_j x_j \int_{t_1}^{t_2} e^{i[(\omega_k+\omega_j)t+(\phi_k+\pi/2)]}\,dt\right\}. \tag{20}$$

If the force and amplitude responses are monochromatic at one and the same frequency ω, corresponding to the kth mode, the work done by the fluid over a period of oscillation can be obtained from Eq. (20) by keeping only the related term, and integrating over a period corresponding to that particular frequency

$$W = F_k x_k \pi \sin(\phi_k). \tag{21}$$

Fig. 16 shows the phase angle between the lift force and the vertical displacement, and how it varies with the reduced velocity for the upstream and downstream cylinders for each of the spacings considered. The phase angle was calculated as the difference between the Fourier coefficient phases of the transverse force and displacement, obtained from the corresponding time history signals. The difference was calculated at the Fourier coefficients corresponding to the prominent response frequencies. This is why in some cases there is more than one point at a given reduced velocity. When there are more than one significant frequencies in the spectra, each point indicates the phase angle of the Fourier mode corresponding to that frequency. The points in this case have different size according to the magnitude of the mode. A bigger point is used for higher amplitude Fourier coefficients.

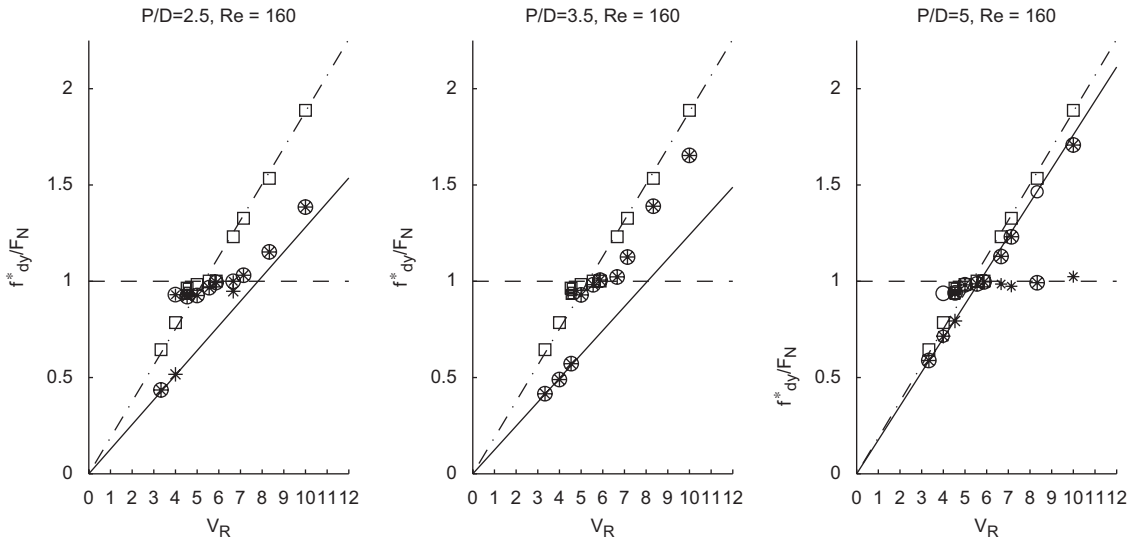

Fig. 14. Frequency of spectral peaks based on vertical displacements: ○, upstream cylinder; ∗, downstream cylinder; □, single cylinder; ——, shedding frequency of corresponding stationary tandem cylinders f_o^{**}; –·–, shedding frequency of the single cylinder f_o^*; – –, natural frequency of structure F_N.

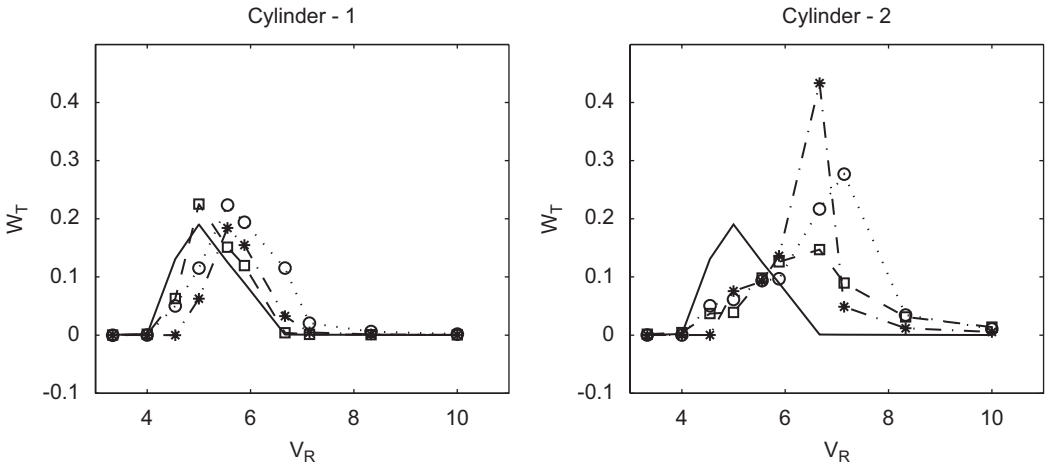

Fig. 15. Total hydrodynamic work acting on the cylinders: · · · ○ · · ·, tandem, $P/D = 2.5$; ---∗---, tandem, $P/D = 3.5$; – –□– –, tandem, $P/D = 5.0$; ——, single cylinder.

For small values of V_R, corresponding to high cylinder natural frequencies f_N (stiff spring), the phase angle is close to zero. The cylinder moves at the direction of the force but is not driven by it and no work is done. For high values of V_R, corresponding to soft spring and small f_N the phase angle is 180°, i.e., the cylinder's deflection is in the opposite direction than that of the force. The net work input over a period is also zero.

There is a range of reduced velocities that the transition from 0° to 180° occurs, and the phase angle obtains intermediate values that yield a net work input with more work done when the phase is about 90°. Work is produced by the component of lift in phase with the vertical velocity. That leads to another important quantity, the 'lift in phase with velocity'. To actually perform the integration, a parametrization in time and change of variable takes place,

$$\oint F\,\mathrm{d}s = \int_{kT}^{(k+1)T} F \underbrace{\left(\frac{\mathrm{d}s}{\mathrm{d}t}\right)}_{\text{velocity}} \mathrm{d}t. \tag{22}$$

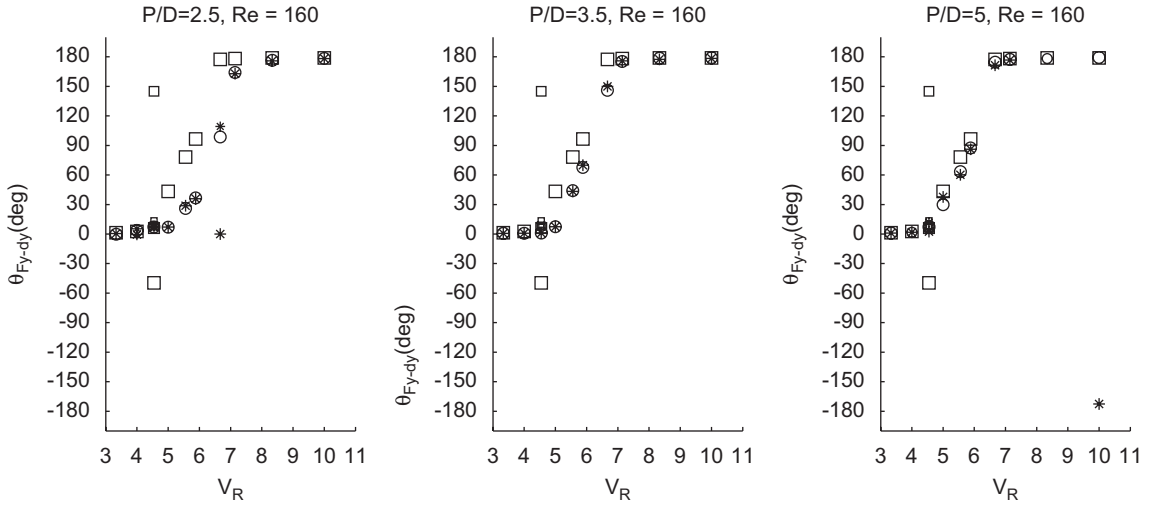

Fig. 16. Phase angle between lift force and transverse displacement. Left: $P/D = 2.5$; middle: $P/D = 3.5$; right: $P/D = 5.0$. ○, upstream cylinder; ∗, downstream cylinder; □, single cylinder.

No hysteresis effect was observed in the phase angle plots. The hysteresis effect occurring on the single cylinder, see Williamson and Roshko (1988), as well as Carberry et al. (2001), is associated with the occurrence of 2P or 2S vortex structures in the wake.

A more detailed discussion on the absence of 2P shedding in the present calculation follows in Section 3.4.

3.4. Flow patterns

From the literature on the vortex-induced vibrations of a single cylinder, see for example Khalak and Williamson (1999), it is expected that the response curve for relatively low mass ratios $\mathcal{O}(1)$–$\mathcal{O}(10)$ involves three branches. Each of the branches is associated with different vortex patterns depending also on $m^*\zeta$, as follows.

(i) An *initial branch* is the first part of the response curve as V_R increases. This branch is associated with a 2S pattern and an almost zero phase angle between lift and transverse response.
(ii) An *upper branch* exhibiting high amplitude oscillations and associated with a 2P shedding pattern. The phase difference is also around zero.
(iii) A *lower branch* where the phase angle between lift force and transverse displacement has become 180°. Part of this regime is associated with 2P shedding and part of it with aperiodic wake, or 'no observed pattern' as termed in Williamson and Roshko (1988).

An important aspect of the response is the hysteretic effects between each part of the curve, as they overlap for a range of V_R. In our two-degree-of-freedom low Reynolds number ($\mathrm{Re} = 160$) simulations we did not observe 2P structures in the flow behind a single cylinder that are associated with those hysteresis effects. As seen in the instantaneous vorticity fields in Fig. 17, for $\mathrm{Re} = 160$ and mass ratios $m^* = 3.0$ and 10.0 at lock-in, there is a wide wake with closely spaced vortices but it is not a 2P wake. At $\mathrm{Re} = 500$ and $m^* = 3.0$ an asymmetric P + S wake structure is observed, as first reported in Papaioannou (2003). The P + S mode in the two-degree-of-freedom oscillations of a single cylinder was independently observed in the numerical simulations of Singh and Mittal (2005) at $\mathrm{Re} = 325$. A P + S structure is observed at higher Reynolds number. However, the validity of the two-dimensional (2-D) simulations is questionable as the Reynolds number increases, although at lock-in the 2-D approximation is expected to be close to reality.

There are several reasons for the absence of the upper branch and 2P shedding in our results. Firstly, the relatively high $m^*\zeta = 0.1$ leading to a Feng-type response without upper branch and a narrower in terms of V_R range lower branch as explained in Khalak and Williamson (1999). Secondly, the 2-D low Reynolds number simulations as also noted in Blackburn et al. (2000). Another likely reason that hysteretic phenomena are not reported in our results is the consistent initial conditions used for each reduced velocity calculation. Additionally for the Reynolds numbers

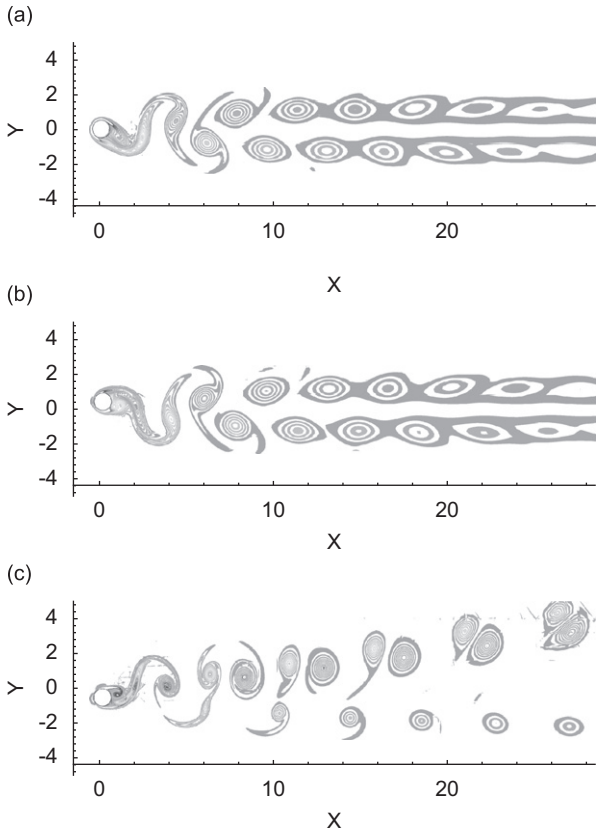

Fig. 17. Instantaneous flow patterns of a single cylinder at lock-in. (a) Re = 160, $m^* = 10.0$, (b) Re = 160, $m^* = 3.0$, (c) Re = 500, $m^* = 3.0$.

examined the hysteresis loops are very narrow as shown in Singh and Mittal (2005), so they would not be captured by our V_R resolution. The two- versus one-degree-of-freedom oscillations is disqualified as a reason, by comparison of one- and two-degree-of-freedom results for the present parameters and Reynolds number. A more detailed discussion on this topic can be found in Papaioannou (2003).

The flow patterns of the tandem cylinders are more complex due to the higher vorticity production and the interaction of the two wakes. For $V_R = 4.0$ the response is on the initial branch for all tandem spacings as well as the single cylinder. As seen in Fig. 11, the flow patterns are similar to Fig. 1 and a 2S like pattern is observed in the wake. Case $P/D = 5.0$ exhibits stronger and horizontally closer spaced vortices compared to the stationary system. At $V_R = 5.555$ the upstream cylinder is at lock-in for all spacings. The high amplitude oscillations result in wide wakes with closely spaced vortices as seen in Fig. 12. However, none of those could be classified as 2P wake. Merging of equal sign vortices takes place on the wake due to their increased strength and short horizontal distance. At $V_R = 8.333$ the small oscillations of the upstream cylinder and larger oscillations of the downstream cylinder allow shedding of vortices in the gap region. In the reattachment regime cases $P/D = 2.5$ and 3.5 the downstream cylinder seems to synchronize its shedding resulting in periodic 2S looking wake. The difference here with the smaller V_R cases is that the phase angle between lift force and y-response is 180°. For $P/D = 5.0$ a complex and not periodic wake results from the combined wakes of the two cylinders.

4. Summary and conclusions

The effect of spacing in the two-degree-of-freedom vortex-induced vibrations of two cylinders in tandem arrangement was studied. The numerical method employed is based on high-order spectral element expansions and a stiffly stable time integration. The motion of the fluid domain boundaries was accommodated by an arbitrary Lagrangian–Eulerian (ALE) scheme.

Three spacings $P/D = 2.5$, 3.5 and 5.0 were considered, each corresponding to a different flow regime when the cylinders are fixed. For the Reynolds number examined ($\mathrm{Re} = 160$), the spacings $P/D = 2.5$ and 3.5 are in the reattachment regime, while the $P/D = 5.0$ is in the binary-vortex regime. The spacing $P/D = 3.5$ is just before the critical spacing. In fact, due to a hysteresis effect, both reattachment and binary-vortex shedding are possible states for this spacing at the examined Reynolds number. The cylinder spacing is found to have the following effects on the response curve of the upstream cylinder. The response curve becomes wider as the cylinders are brought closer to each other, i.e., there is a wider range of reduced velocities (V_R) for which the upstream cylinder exhibits high amplitude oscillations. There is also a shift of the response curve toward higher reduced velocities. The shift is explained in terms of the change in the natural shedding frequency (f_o^{**}) for different spacings of the fixed cylinders' system. As the spacing increases into the binary-vortex regime ($P/D = 5.0$ case), the upstream cylinder is almost unaffected by the presence and oscillation of the downstream. Its response is very close to the single cylinder both in terms of size and shift along the V_R axis compared to the other spacings. The response curve of the downstream cylinder is shifted toward higher values of the reduced velocity compared to the upstream for all examined spacings. This shift is attributed to the *shielding effect*.

The effect of spacing is also manifesting itself in the spectra of the responses. All the peaks in the response spectra are identified and interpreted in terms of three prominent frequencies, their super-harmonics and differences among them. The first is the natural frequency of the cylinder f_N. The second is the shedding frequency of the corresponding stationary tandem system f_o^{**}. Finally, the third significant frequency is the shedding frequency of the single stationary cylinder f_o^*. For all spacings, at lock-in, the significant frequency is f_N as expected. At non-lock-in frequencies, however, the effect of spacing is masked into response peaks at the frequency f_o^{**}. For spacings $P/D = 2.5$ and 5.0, at every V_R not corresponding to lock-in, there is at least one peak at the corresponding f_o^{**} and possibly additional ones at f_N. For the case $P/D = 3.5$ and V_R higher than lock-in there is deviation from that behavior, with the response frequencies higher than f_o^{**} and closer toward f_o^*. This is attributed to the special, hysteretic with respect to spacing, behavior of the corresponding stationary system where both reattachment and binary-vortex regimes can be realized, yielding of course different values of f_o^{**} for this case.

The hysteresis effect, with respect to the reduced velocity, and 'upper branch' known to exist for the single oscillating cylinder was not observed in this study. This is attributed to the mass-damping parameter, Reynolds number and 2-D calculations.

Acknowledgments

This work was supported by the Office of Naval Research (ONR, T.F. Swean). Computations were performed at the Naval Oceanographic Office (NAVOCEANO) Major Shared Resource Center (MSRC) and at NCSA University of Illinois at Urbana-Champaign. The last author would also like to acknowledge support by ONR (T.F. Swean).

Appendix A. Verification of results

Given the number of parameters that play a role in the problem, (m^*, ζ, V_R, Re, P/D) a one-to-one comparison with experimental or other numerical results is not always available. Another difficulty in regard to quantitative comparison with experimental results is that for most experimental techniques the Reynolds number increases along with the reduced velocity. While in numerical results reduced velocity changes by changing only the natural frequency of the cylinders f_N. In lack of a direct comparison for the chosen parameters of the two-degree-of-freedom vortex-induced oscillations of tandem cylinders, the verification process is divided in several sub-stages. First, we verify the single stationary cylinder case, and then the stationary tandem cylinders and also a single cylinder in two-degree-of-freedom flow-induced oscillations. Finally, we provide a comparison of the results for a single case run on two completely different computational meshes to prove the used meshes provide adequate accuracy.

A.1. Single stationary cylinder

The calculated nondimensional shedding frequency of a single cylinder at $\mathrm{Re} = 100$, 160 and 200 is compared in Table A1 with the corresponding experimentally obtained by Williamson (1988). The results agree within less than 4% in all three Reynolds numbers examined. It should be noted here that for higher Reynolds numbers three-dimensionalities become increasingly important as discussed in detail in Papaioannou et al. (2006).

Table A1
Comparison of the calculated shedding frequency (f_o^*) of a single stationary cylinder with experimental results

Re	100	160	200
Present work	0.170	0.188	0.200
Williamson (1988)	0.164	0.186	0.196

Table A2
Comparison of drag coefficient and shedding frequency of stationary tandem cylinders among various two-dimensional numerical studies

Work	Re	P/D	$\overline{C_{D1}}$	$\overline{C_{D2}}$	St
Present work (2-D)	100	3.0	1.16	0.05	0.116
Sharman et al. (2005)	100	3.0	1.111	−0.02	0.110
Present work (2-D)	100	3.5	1.16	0.05	0.116
Sharman et al. (2005)	100	3.5	1.106	0.03	0.110
Present work (2-D)	100	4.0	1.31	0.75	0.152
Sharman et al. (2005)	100	4.0	1.274	0.705	0.148
Present work (2-D)	200	3.0	1.02	−0.12	0.128
Meneghini et al. (2001)	200	3.0	1.00	−0.08	0.125
Present work (2-D)	200	3.5	1.27	0.40	0.174
Slaouti and Stansby (1992)	200	3.5	0.85	−0.18	0.12

$\overline{C_{D1}}$: upstream cylinder, $\overline{C_{D2}}$: downstream cylinder.

A.2. Stationary tandem cylinders

Table A2 compares stationary tandem cylinder results presently obtained, with corresponding 2-D numerical results in the literature. The choice of literature data was made based on availability of results at the corresponding spacing and Reynolds number. The results match exactly in up to two significant digits in most quantities, with the only exception the results of Slaouti and Stansby (1992) who used the Lagrangian in nature random vortex method. The discrepancy may be due to the spacing of the comparison which is just about the critical spacing for that Reynolds number where there are hysteretic effects and big jumps in the values of forces. Sharman et al. (2005) applied a collocated unstructured computational fluid dynamics (CUCFD) method. The domain was divided by cell-centered unstructured mesh into triangular control volumes. The velocity and pressure were stored at the cell centroids (collocated variable arrangement). The momentum and the pressure-correction equations were then solved iteratively using the SIMPLE algorithm. In Meneghini et al. (2001) a fractional step method was used. The calculations were carried out on three-node unstructured meshes by means of a Poisson's equation for the pressure and a Taylor–Galerkin formulation for the intermediate velocity.

A.3. Vortex-induced vibrations of a single cylinder

In Fig. A1 we show a comparison between the presently obtained results for a single cylinder in two-degree-of-freedom vortex-induced oscillations, with those of Singh and Mittal (2005) who employed a numerical method based on space–time finite elements. Their data were obtained for somewhat different parameters. For the drag coefficient the Reynolds number was 100 and there was no damping ($\zeta = 0$). On the other hand, the mass ratio $m^* = 10$ was the same, and two-degree-of-freedom oscillations were numerically studied. The zero damping parameter leads to higher oscillations and drag coefficients compared to ours. We obtained two extra points at $\zeta = 0.0$. As expected, one of these points, $V_R = 5.88$, in the synchronization range exhibits higher drag than the corresponding at $\zeta = 0.01$, and it is closer to the results of Singh and Mittal (2005).

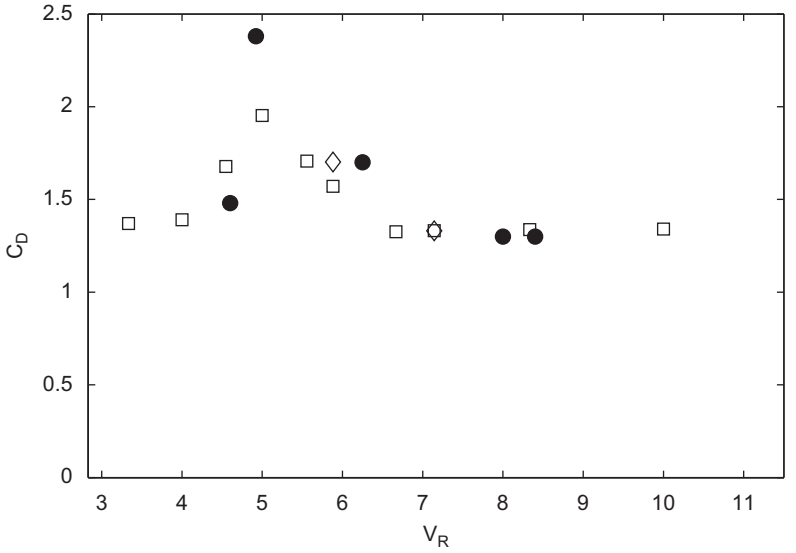

Fig. A1. Comparison of drag coefficient of single oscillating cylinder. □, Present study ($m^* = 10.0$, $\zeta = 0.01$, Re = 160); ◇, present study ($m^* = 10.0$, $\zeta = 0.00$, Re = 160); ●, Singh and Mittal (2005) ($m^* = 10.0$, $\zeta = 0.00$, Re = 100).

Table A3
Comparison of response and force statistics between two different meshes for tandem cylinders $P/D = 3.5$ at Re = 160 and reduced velocity $V_R = 6.67$

Mesh	Order	Mesh area	N_{Elem}	N_{Tri}	N_{Quad}
A	5	$[-10.5, 42.5] \times [-12, 12]$	3526	3526	0
B	7	$[-12.5, 45.5] \times [-12, 12]$	1816	790	1026
	Cylinder	x-Amplitude	y-Amplitude	$\overline{C_D}$	C'_L
A	Upstream	0.0042	0.48	1.34	0.12
B	Upstream	0.0046	0.48	1.33	0.11
A	Downstream	0.0225	1.64	1.49	0.54
B	Downstream	0.0222	1.72	1.54	0.45

A.4. Mesh quality verification

The results presented so far are based on the computational meshes presented in Section 2.2 and Table 2. The spectral element methodology allowed us to reach adequate resolution by increasing the polynomial order of each element without having to change the number of elements, a process known as *p-refinement*. More detailed results on these studies for each of the meshes can be found in Papaioannou (2003). To re-confirm the adequacy of the selected computational mesh, one case was recomputed with a completely different mesh consisting of only triangular elements with fifth-order polynomial bases, or equivalently $(p + 1)p/2 = 15$ modes per element. Comparisons of the two meshes and the obtained results are presented in Table A3. It should be noted that the total degrees of freedom in the triangular mesh is about 35% less than those of the hybrid mesh actually used in the study. The results of the upstream cylinder are almost identical. For the downstream cylinder oscillation amplitudes and drag force are all below 5% accuracy, but the C'_L is up to 20% different.

References

Allen, D., Henning, D., 2003. Vortex-induced vibration current tank tests of two equal-diameter cylinders in tandem. Journal of Fluids and Structures 17, 767–781.

Assi, G., Meneghini, J., Aranha, J., Bearman, P., Casaprima, E., 2006. Experimental investigation of flow-induced vibration interference between two circular cylinders. Journal of Fluids and Structures 22, 819–827.

Bearman, P., 1984. Vortex shedding from oscillating bluff bodies. Annual Review of Fluid Mechanics 16, 195–222.

Blackburn, H., Govardhan, R., Williamson, C., 2000. A complementary numerical and physical investigation of vortex-induced vibration. Journal of Fluids and Structures 15, 481–488.

Blevins, R., 1994. Flow-induced Vibrations. Van Nostrand Reinhold Company, New York.

Brika, D., Laneville, A., 1999. The flow interaction between a stationary cylinder and a downstream flexible cylinder. Journal of Fluids and Structures 13, 579–606.

Carberry, J., Sheridan, J., Rockwell, D., 2001. Forces and wake modes of an oscillating cylinder. Journal of Fluids and Structures 15, 523–532.

Donea, J., Giuliani, S., Halleux, J., 1982. An arbitrary Lagrangian–Eulerian finite element method for transient dynamic fluid-structure interactions. Computer Methods in Applied Mechanics and Engineering 33, 689–723.

Hover, F., Triantafyllou, M., 2001. Galloping response of a cylinder with upstream wake interference. Journal of Fluids and Structures 15, 503–512.

Hughes, T., Liu, W., Zimmermann, T., 1981. Lagrangian–Eulerian finite element formulation for incompressible viscous flows. Computer Methods in Applied Mechanics and Engineering 29, 329–349.

Igarashi, T., 1981. Characteristics of the flow around two circular cylinders arranged in tandem (first report). Bulletin of the Japanese Society of Mechanical Engineers 24, 323–331.

Jester, W., Kallinderis, Y., 2003. Numerical study of incompressible flow about fixed cylinder pairs. Journal of Fluids and Structures 17, 561–577.

Karniadakis, G., Sherwin, S., 2005. Spectral/hp Element Methods for CFD. Oxford University Press, Oxford, UK.

Karniadakis, G., Israeli, M., Orszag, S., 1991. High-order splitting methods for the incompressible Navier–Stokes equations. Journal of Computational Physics 97, 414–443.

Khalak, A., Williamson, C., 1999. Motions, forces and mode transitions in vortex-induced vibrations at low mass-damping. Journal of Fluids and Structures 13, 813–851.

Lam, K., To, A., 2003. Interference effect of an upstream larger cylinder on the lock-in vibration of a flexibly mounted circular cylinder. Journal of Fluids and Structures 17, 1059–1078.

Laneville, A., Brika, D., 1997. The power imparted by wind to a flexible circular cylinder in the wake of another stationary cylinder. IEEE Transactions on Power Delivery 2, 398–405.

Mahir, N., Rockwell, D., 1996. Vortex formation from a forced system of two cylinders—part i: tandem arrangement. Journal of Fluids and Structures 10, 473–489.

Meneghini, J., Saltara, F., Siqueira Jr., J.F., 2001. Numerical simulation of flow interference between two circular cylinders in tandem and side-by-side arrangements. Journal of Fluids and Structures 15, 327–350.

Mittal, S., Kumar, V., 2001. Flow-induced oscillations of two cylinders in tandem and staggered arrangements. Journal of Fluids and Structures 15, 717–736.

Naudascher, E., Rockwell, D., 2005. Flow-induced Vibrations: An Engineering Guide. Dover Publications, New York.

Newmark, N., 1959. A method of computation for structural dynamics. Journal of the Engineering Mechanics Division pp. 67–94.

Papaioannou, G., 2003. A numerical study of flow-structure interactions with application to flow past a pair of cylinders. Ph.D. Thesis, Massachusetts Institute of Technology.

Papaioannou, G., Yue, D., Triantafyllou, M., Karniadakis, G., 2006. Three-dimensionality effects in flow around two tandem cylinders. Journal of Fluid Mechanics 558, 387–413.

Sarpkaya, T., 1979. Vortex-induced oscillations a selective review. Journal of Applied Mechanics 46, 241–258.

Sharman, B., Lien, F., Davidson, L., Norberg, C., 2005. Numerical predictions of low Reynolds number flows over two tandem circular cylinders. International Journal for Numerical Methods in Fluids 47, 423–447.

Singh, S., Mittal, S., 2005. Vortex-induced oscillations at low Reynolds numbers: hysteresis and vortex-shedding modes. Journal of Fluids and Structures 20, 1085–1104.

Slaouti, A., Stansby, P., 1992. Flow around two circular cylinders by the random-vortex method. Journal of Fluids and Structures 6, 641–670.

Williamson, C., 1988. Defining a universal and continuous Strouhal–Reynolds number relationship for the laminar vortex shedding of a circular cylinder. Physics of Fluids 31, 2742–2744.

Williamson, C., Roshko, A., 1988. Vortex formation in the wake of an oscillating cylinder. Journal of Fluids and Structures 2, 355–381.

Zdravkovich, M., 1985. Flow induced oscillations of two interfering circular cylinders. Journal of Sound and Vibration 101, 511–521.

Zdravkovich, M., 1987. The effect of interference between circular cylinders in cross flow. Journal of Fluids and Structures 1, 239–261.